Studies of Li-rod based muon ionization cooling channel

A.N. Skrinsky[a], T.V. Zolkin*[,b]

[a] *Budker Institute of Nuclear Physics, 11 akademika Lavrentieva prospect, Novosibirsk, 630090 Russia*

[b] *The University of Chicago, 5720 South Ellis Avenue, Chicago IL, 60637-1434 USA*

Abstract

The muon ionization cooling channel based on lithium rods (Li-rod) has been under consideration since the 1990s (1). Features of muon beam motion are discussed, namely the influence of non-paraxiality of motion and transverse-longitudinal coupling. The inclusion of an emittance exchanger to the cooling channel can result in the cooling of all degrees of freedom. The appropriate beam parameters for emittance exchange procedure and their dependence on transverse emittance and beam longitudinal parameters are discussed. Most simulations of muon beam cooling were performed using the specially developed software LyRICS (Lithium Rod Ionization Cooling Simulation); a comparison between its results and the predictions of a linear model serves both to examine the simulation code and to determine the contribution of non-paraxiality to the beam motion. An additional comparison with a simulation based on G4beamline code is also presented. More complete consideration of longitudinal cooling and emittance exchange procedure will be presented in future work. For numerical examples, we used muons around 200 MeV total energy since such energy is close to optimal.

Key words: muon collider, ionization cooling, lithium rod, "head-tail" rotation, LyRICS, emittance exchange

*Corresponding author.

Email addresses: skrinsky@inp.nsk.su (A.N. Skrinsky), zolkin@uchicago.edu (T.V. Zolkin)

1. Introduction

One of the most (or, maybe, just the most) important steps that enabled progress in Elementary Particle Physics was the development and practical implementation of colliding beams over 50 years ago, that led to the construction of particle colliders. Higher energy and higher productivity (luminosity) of colliders to further increase the sensitivity and precision of collider experiments are important for any further progress in HEP.

The Large Hadron Collider (4), which has recently started its operation near Geneva, Switzerland, is currently the energy frontier facility. It is designed, constructed and operated by a team of physicists from leading high energy physics laboratories all over the world. The LHC will provide high luminosity proton-proton collisions with a maximum center-of-mass energy of up to 14 TeV.

A proton-proton collision at very high energy is equivalent to a collision of its fundamental constituents with an effective energy of about 1/6 of the initial proton energy, though with a very wide energy spectrum. As a result of this complex collision, analysis of experimental data and extraction of properties of fundamental interactions become difficult and the result is not always unambiguous.

Therefore, it is of critical importance to have a possibility for an independent study of high energy processes in collisions with a well-determined initial state. At moderately high energies (up to about 1 TeV center-of-mass energy) linear electron-positron colliders could solve the problem acceptably well. However, in order to reach sufficiently high luminosity, bunches of particles of both high intensity and high density are required. Such high-density e^- (e^+) bunches produce very high focusing radial electric and azimuthal magnetic fields, so primary particles emit too many photons. The effect can be substantially reduced with the use of wide but very thin bunches of the same transverse cross section. However, even in this case at center-of-mass energies of 1 TeV the effective energy spread reaches several tens of percent. The use of electron-electron collisions instead leads to the strong repulsion, which results in orders of magnitude lower luminosity.

The source of this problem is in smallness of the electron mass, as the emitting power in a collision is proportional to E^2/m^4. The effect can be practically suppressed if heavier leptons are used. The only heavier lepton with acceptably long lifetime is a muon whose mass is a factor of 200 higher than that of an electron. The muon lifetime is 2.2 μs in its rest frame and

rises proportionally to its total energy in the laboratory frame. As a result, one can expect up to 1000 bunch collisions in a high-field cyclic collider prior to the muon decay. Thus in a collider of a given perimeter and guiding magnetic field, use of muons instead of protons allows one to study fundamental interactions at six times higher energy and under much cleaner conditions (initial particles are well determined and effective monochromaticity of collisions is much, much better). Muon colliders are believed to be the main hope (the only one?) for a precision study of fundamental interactions at a several TeV center-of-mass energy scale.

However, there are several key technologies required for the successful construction of a muon collider which are still not fully developed. First of all, it is necessary to cool down the muon beams to reduce the 6-dimensional emittances by 5–6 orders of magnitude while preserving the intensity as carefully as possible. Such a progress in muon cooling is a must to reach sufficient luminosity.

The most promising way for muon beam cooling is to use ionization energy losses in some dense matter with a consequent compensation of lost energy (and longitudinal momentum) via the RF field (2; 3). Much effort is being invested in many research laboratories worldwide to develop and study various cooling schemes both analytically and using computer simulation (5; 6; 7; 8; 9; 10; 11). Recently, preparation started for an experimental study of some cooling techniques (12; 13; 14).

This article covers more carefully the study of a cooling channel based on Li-rods which provide muon energy losses due to ionization and simultaneously strong transverse focusing by carrying a very high current. While its technical realization is still in development, Li-rod usage may be a way to make the strongest focusing which is essential for the final cooling stage. Predominantly, this article focuses on a muon motion analysis in a single Li-rod, which is a core of this cooling scheme, and not on a whole beamline. Different features of transverse and longitudinal muon beam motion through rods are presented in Sections 4 and 5 respectively (such as nonparaxiality and transverse-longitudinal coupling). Also, optimal parameters for the emittance exchange procedure (which can upgrade the cooling to all degrees of freedom) are determined in the Sections 5.1. At the end of this paper one can find two appendixes where the linear models for transverse and longitudinal motion are investigated in detail. The comparison between different simulations and linear model predictions are presented.

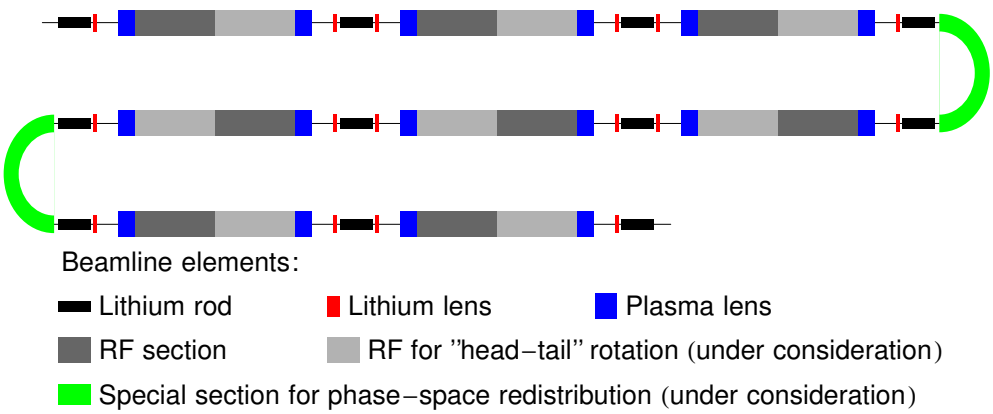

Figure 1: Beamline for final cooling stage.

2. Cooling scheme under consideration

The proposed cooling channel, which is based on Li-rods alternating with RF cavities, is presented in Fig. 1. The matching between main elements is realized by the cascade of lithium and plasma lenses (7): the short lithium lenses (strong in comparison with plasma ones) make the beta-function a few times larger at the exit of lithium rods (smaller at the entrance) and weaken the low-aberration functioning of plasma lenses, which have longer focal lengths. An example of beta-function behavior along with parameters for one period of this cooling scheme are presented in Fig. 2 and Table 1 respectively. Abbreviations used in Table 1 are:

1. Li-r. — lithium rod
2. D.S. — drift space
3. Li l. — lithium lens
4. Pl l. — plasma lens
5. RF — RF cavity
6. E — energy at the exit of element $[MeV]$
7. β — beta-function at the exit of element $[cm]$
8. H — magnetic field on the surface of element $[10^4 \times Gauss]$
9. I — current through the element $[10^5 \times A]$
10. L — length of element $[cm]$
11. D — diameter of element $[cm]$

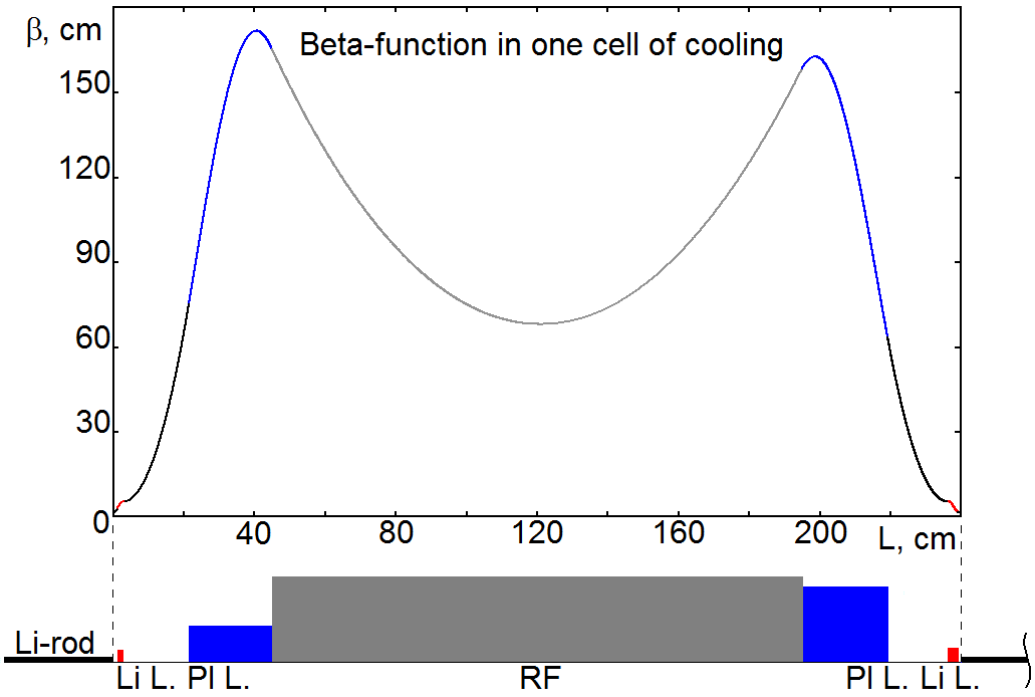

Figure 2: Example of the beta-function behavior in one period of the cooling channel.

	Li-r.	D.S.	Li l.	D.S.	Pl. l.	RF	Pl. l.	D.S.	Li l.	D.S.	Li-r.
E	190	190	190	190	190	220	220	220	220	220	190
β	1.11	2.52	5	75.28	165	158	63.19	5	1.39	1.1	1
H	20	—	14.7	—	0.31	—	0.79	—	13.9	—	20
I	5	—	7.81	—	0.5	—	2.6	—	8.18	—	4
L	30	1.25	1.63	18.7	23.37	150	24.6	17.05	2.84	0.56	30
D	1	—	2.14	—	6.3	—	13.32	—	2.34	—	0.8

Table 1: Example of element parameters for one period of the cooling channel.

The scheme specified above can provide only 4-D cooling for transverse degrees of freedom while the longitudinal degree of freedom undergoes heating. For a 6-D cooling realization it is possible to use a special section, such as an emittance exchanger, after several periods (lithium rod and RF cavity pairs). Such a section should redistribute phase-space from the longitudinal degree of freedom to transverse ones, which helps to further the cooling process (this part of the cooling scheme will be studied in the upcoming article).

As will be shown in Section 5.2, the non-paraxiality of motion results in a higher rate of heating of the longitudinal degree of freedom in comparison with predictions of a paraxial model (up to 2 times). An additional RF cavity, which rotates a beam in the $(cdt, dE/E_{eq})$ plane by an angle of pi, can be placed after a main one to suppress this undesirable effect.

3. Beam motion simulation

The multi-purpose software "Lithium Rod Ionization Cooling Simulation" (LyRICS) has been developed for a study of a scheme of final cooling for muon beams (based on consequent lithium rods). It can simulate the 6-dimensional motion of a muon beam through matter including such effects as non-paraxiality, dissipation and stochastic processes like scattering or fluctuations of energy losses. Also LyRICS allows one to simulate the motion in matching sections based on lithium and plasma lenses, including acceleration in RF cavities (taking into account transverse focusing due to transverse components of RF-fields) and estimate its technical parameters.

4. Transverse motion

In the paraxial case, the evolution of the second moments of the beam $< x^2 >$, $< x'^2 >$, $< xx' >$ and the transverse emittance ε_{tr} is sufficiently simple and can be described analytically (see Appendix A). Examples of their behavior are presented in Fig. 3. Each of these quantities is asymptotic to a certain constant value with respect to the longitudinal coordinate s (see Appendix A eq. (9)) and tend to the limit from above (below) if its initial value is bigger (smaller) than equilibrium one. In the most general case, when the initial values of the second moments are unmatched with the optical functions of the cooling channel, they are damped with oscillations (grey dashed lines on the graph). Despite the fact that in both cases the cooling

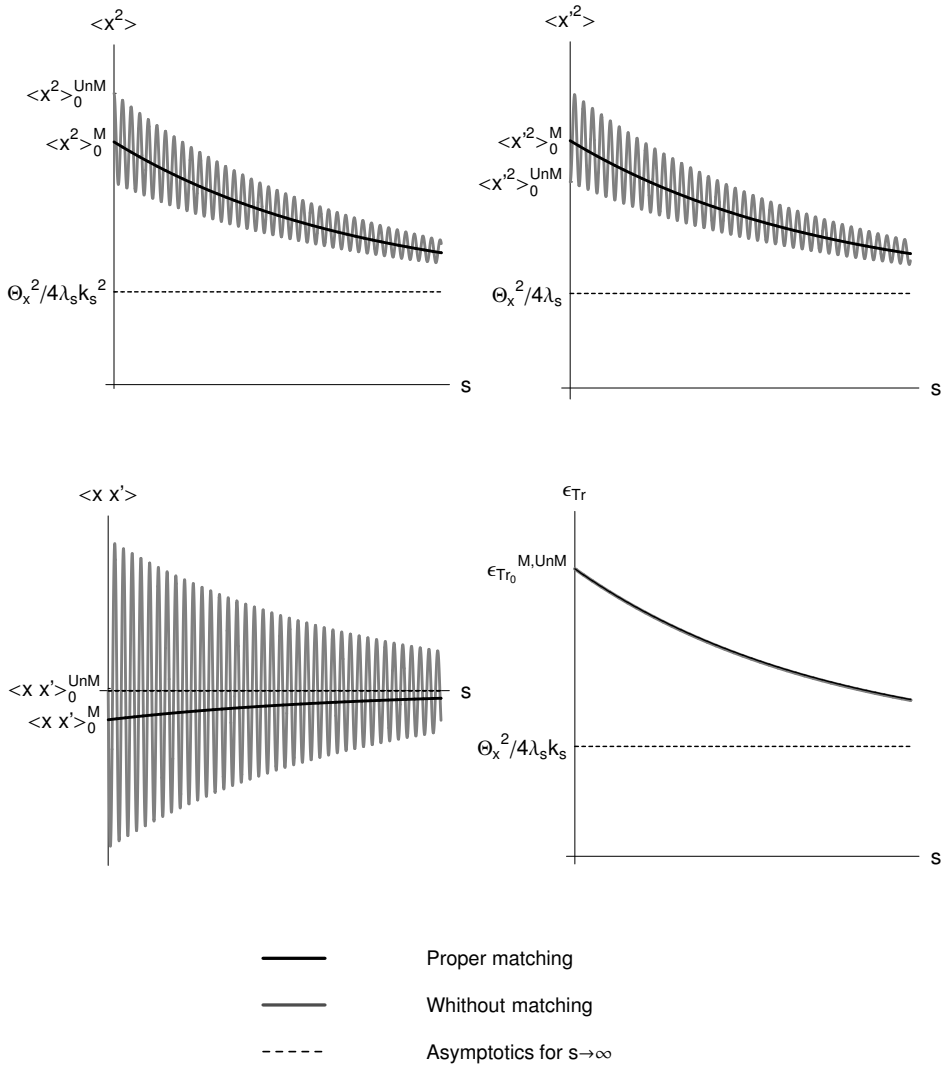

Figure 3: Behavior of the second moments of the beam and transverse emittance due to ionization cooling in the cases of matched initial conditions (black curves and values marked by "M" label) and unmatched ones (gray curves and values marked by "UnM" label).

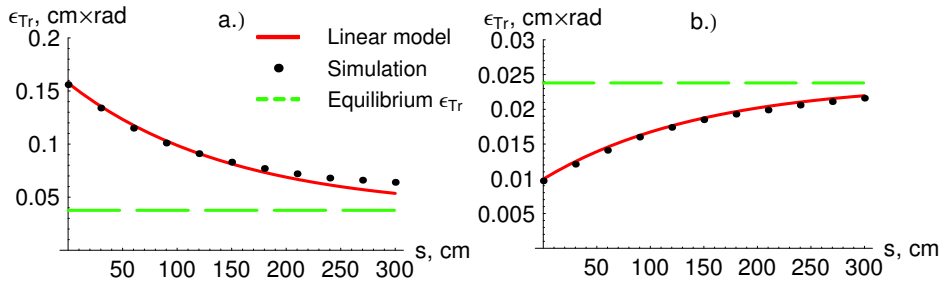

Figure 4: Linear model of transverse motion compared to simulation in the cases of a) large initial transverse emittance and b) small one.

rate is the same, there is no doubt that these oscillations are undesirable because they can lead to additional particle losses on the physical aperture and should be avoided (see Appendix A eq. (12)).

4.1. Comparison of linear model and simulation

A comparison between the simulation results and the predictions of a paraxial linear model is presented below, with specific examples shown in Fig. 4 for two different values of the initial transverse emittance. The simulation was made for ten consecutive lithium rods similar to that considered in Section 2 (each has a length of 30 cm and a 2×10^5 $Gauss$ limitation for a field on its surface). Particle motion in the matching and acceleration sections were simulated as ideal thin transformations such that the full energy of a beam at the entrance to each rod is equal to 220 MeV and the second moments are matched with the channel optics. The beam energy used in the linear model is about 205 MeV, corresponding to the simulated beam energy. It turns out that this relatively simple analytical model agrees with simulation to high precision, with a discrepancy of less than 5%.

To determine in detail how longitudinal motion affects the cooling of transverse degrees of freedom, beam passage through a single rod was examined for multiple values of initial longitudinal emittance[1] with a fixed initial transverse emittance. It has been found that only in cases of relatively small transverse emittance close to the equilibrium value or substantial initial energy spread (more than 10%) is there a small decrease in the rate of cooling

[1]Or more exactly, the initial position of the beam in the $(c\Delta t, \Delta E/E_{eq})$ plane.

compared (around 5%) to the linear model. This confirms that the influence of longitudinal motion on the cooling of the transverse degrees of freedom is indeed small. As expected, the dependence of transverse cooling on the beam parameter $c\Delta t$ was not found.

5. Longitudinal motion

Similar to transverse motion, the longitudinal motion of the beam in matter can be described analytically by a linear approach (see Appendix B). The heating of longitudinal moments occurs by two processes: antidamping under the action of ionization friction and "diffusion" — a fluctuation of ionization losses.

In this model the behavior of the root-mean-square energy spread (eq. (26)) can be described using a certain characteristic value

$$\left(\Delta E/E_{eq}\right)^2_{ch} = -\Theta^2_{dE/E}/4\lambda_t. \tag{1}$$

If the initial energy spread in a beam is larger than this value, an exponential growth of the root-mean-square energy spread by antidamping is observed. Vice versa, for the case when $\langle\left(\Delta E/E_{eq}\right)^2\rangle_0 < \left(\Delta E/E_{eq}\right)^2_{ch}$, this longitudinal second moment has an extremely fast growth described by diffusion initially (the smaller the initial value of the energy spread, the faster the growth), which becomes exponential. Note that, the value of the longitudinal density increment λ_t is assumed to be negative, while the value of the transverse decrement λ_s is positive. The similar quantity $\Theta^2_x/4\lambda_s$, for the case of the transverse motion, refers to the equilibrium angular spread determined by the competition of damping and diffusion processes. Numerical examples of the evolution of the root-mean-square energy spread is presented in Fig. 5 (top left plot), where the average full energy is chosen as 205 MeV.

The behavior of the root-mean-square spread of the arrival time can be analyzed in a similar manner — one can determine another characteristic value $\left(c\Delta t\right)_{ch}$, which corresponds to a "boundary" between behaviors dominated by the two considered processes. In contrast to $\left(\Delta E/E_{eq}\right)_{ch}$, however, it will be a function of all initial data $\left(\langle\left(c\Delta t\right)^2\rangle_0, \langle\left(\Delta E/E_{eq}\right)^2\rangle_0, \langle\left(c\Delta t\right)\left(\Delta E/E_{eq}\right)\rangle_0\right)$. The spread of the arrival time has asymptotics which depend on $\langle\left(\Delta E/E_{eq}\right)^2\rangle_0$ only, regardless of the initial value $\langle\left(c\Delta t\right)^2\rangle_0$:

$$\left\langle\left(c\Delta t\right)^2\right\rangle\Big|_{t\to\infty} = \frac{c^2}{\gamma^2_{eq}}\left(\left\langle\left(\frac{\Delta E}{E_{eq}}\right)^2\right\rangle_0 - \frac{\Theta^2_E}{4\lambda_t}\right)\frac{e^{-4\lambda_t t}}{4\lambda^2_t}. \tag{2}$$

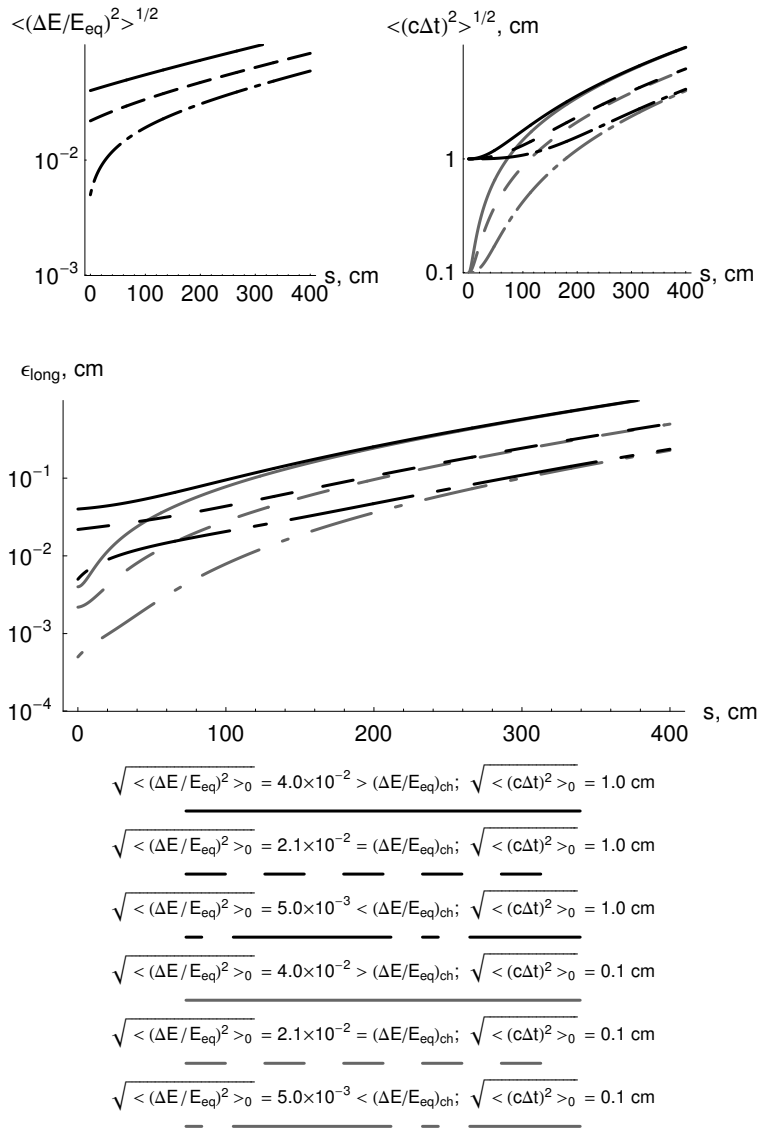

Figure 5: Evolution in matter of the longitudinal second moments $\langle (c\Delta t)^2 \rangle$ and $\langle (\Delta E/E_{eq})^2 \rangle$ as well as the longitudinal emittance ε_{long} for different initial values.

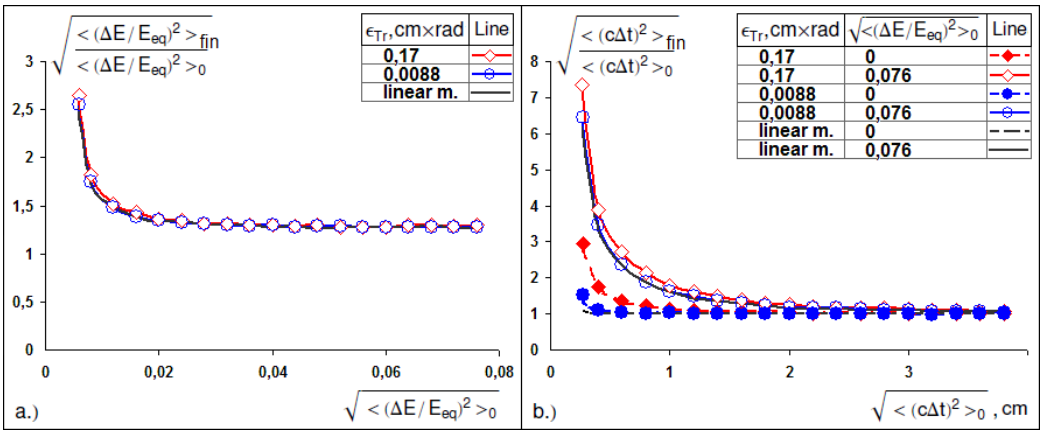

Figure 6: Growth of beam longitudinal parameters after single rod passage under different initial conditions in comparison with a linear model (denoted by "linear m.").

Several examples of the behavior of $\langle(c\Delta t)^2\rangle$ are shown in Fig. 5 (top right) for different values of $\langle(c\Delta t)^2\rangle_0$ and $\langle(\Delta E/E_{eq})^2\rangle_0$ (the value of $\langle(c\Delta t)\,(\Delta E/E_{eq})\rangle_0$ is equal to zero for simplicity for all cases). The evolution of the longitudinal emittance ε_{long} is given at the bottom of this figure for all considered sets of initial beam second moments.

5.1. Comparison of linear model and simulation

The same analysis of beam passage through one rod with variation of the initial conditions (such as the initial beam position in the $(c\Delta t, \Delta E/E_{eq})$ plane and ε_{tr} initial), which has been used in Section 4.1, is also useful for describing the dependence of longitudinal emittance heating on transverse beam parameters.

The growth of $\langle(\Delta E/E_{eq})^2\rangle$ (the ratio of the final root-mean-square energy spread upon the exit of a lithium rod to that at the entrance) is shown in Fig. 6 a.). As expected, it is independent of the transverse beam parameters, even for large values (though undoubtedly these parameters are limited from above to values reasonable for this cooling scheme).

In contrast, the growth of $\langle(c\Delta t)^2\rangle$ conforms to the linear model prediction with confidence only in the case of small transverse emittance (lines with circle symbols in Fig. 6 b.)); the increment of the spread in the arrival time upon the exit of the rod grows with the transverse emittance (at fixed initial parameters, namely, $\langle(c\Delta t)^2\rangle_0$ and $\langle(\Delta E/E_{eq})^2\rangle_0$). This effect is demonstrated for two cases with different initial energy spreads (solid and

dashed lines which refer to large and small values of $\langle(\Delta E/E_{eq})^2\rangle_0$, respectively). This too is a result of non-paraxiality of motion — the presence of particles with big angles entails a significant increase in the paths they take, relative the equilibrium one.

As mentioned above, for the 6-D type of cooling channel, the final value of full emittance is determined by the equilibrium value of the transverse emittance (eq. 14) and how much phase-space volume is redistributed from the longitudinal to transverse degrees of freedom during cooling. Therefore, the wish to redistribute as much as possible is natural, but there is a certain limitation: if the longitudinal second moment values are too small then diffusion begins dominating and longitudinal heating goes faster, which can even lead to full 6-D emittance heating. In Fig. 7, two sketches of cooling with redistribution demonstrate how an excessive redistribution (right column of figures) can slow down 6-D cooling. Therefore, a proper value for the longitudinal emittance after redistribution, or rather a beam position on the $(c\Delta t, \Delta E/E_{eq})$ plane, and the dependence of that value on the transverse motion should also be determined.

By scanning the $(c\Delta t, \Delta E/E_{eq})$ plane of initial beam parameters, one can determine the region of parameters optimal for cooling as a function of the transverse phase-space (for a certain length of rod). An example of such a scan is presented in Fig. 8 for the 30-cm rod with a 2×10^5 $Gauss$ limitation for the field on its surface. The "0" emittance case in Fig. 8 b. refers to a simulation where transverse motion was completely removed and, therefore, the obtained region is very close to that predicted by the linear model. One can therefore conclude that while transverse motion is independent of longitudinal parameters, longitudinal motion is strongly influenced by transverse beam parameters.

5.2. "Head-tail" rotation

Upon studying the cooling process as a whole, simulations show that the longitudinal emittance grows faster than the linear model predicts (up to two times).

A study of the distribution of particle arrival times during the cooling process reveals its deformation after passing through a few rods (a numerical example is presented in Fig. 9 bottom). There are three main differences between the initial and final distributions. First of all, the packet spreads faster than predicted by the linear model. Also, a long tail forms asymmetrically as a result of lagging particles. The third difference, which is a direct

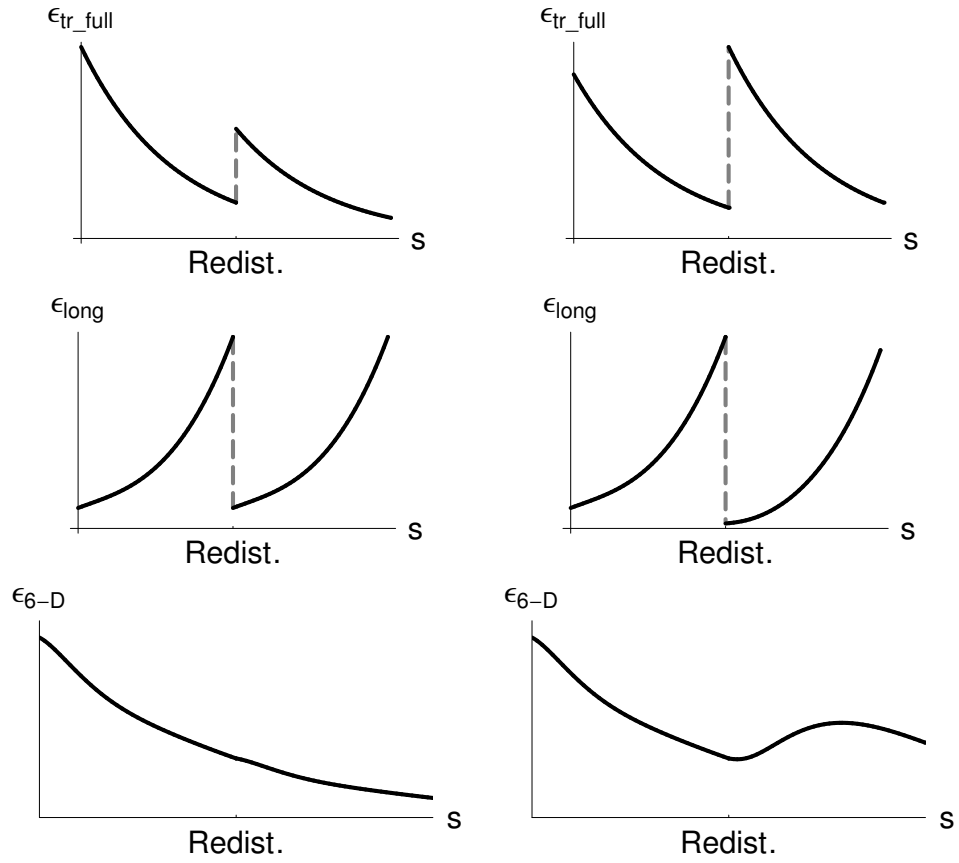

Figure 7: Behavior of full transverse, longitudinal and 6-D emittances as functions of the length passed in matter during cooling with the optimal redistribution from the longitudinal to transverse degrees of freedom (left column) and excessive redistribution with undesirable full emittance increment (right column). The redistribution is shown as a thin ideal process by dashed gray lines.

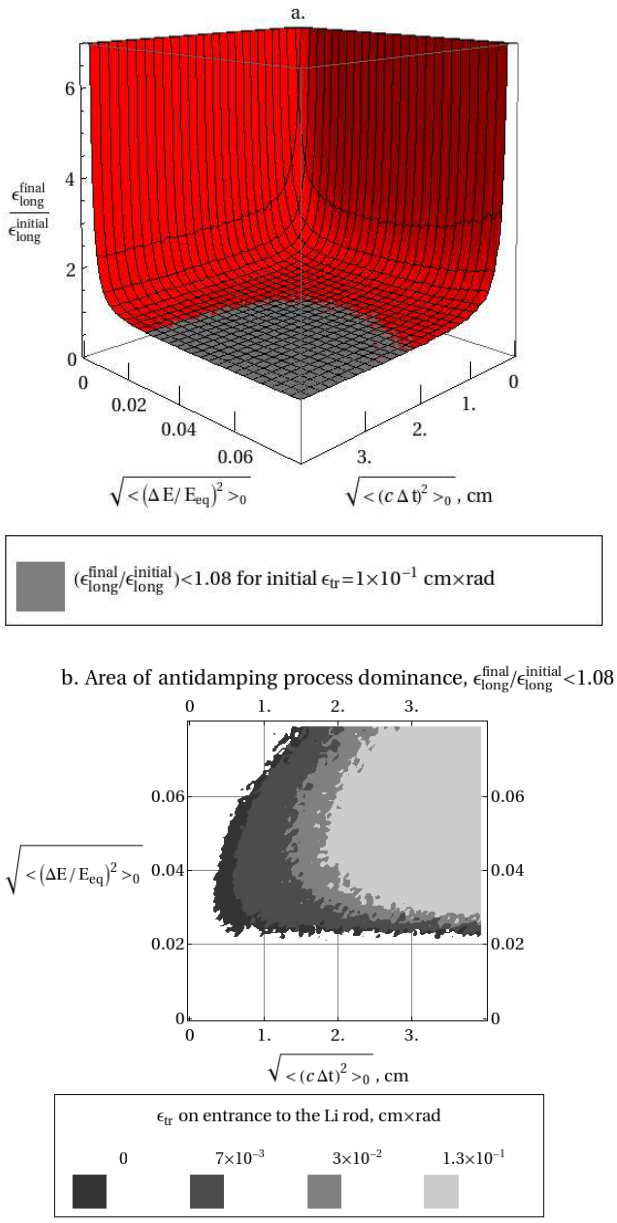

Figure 8: a. Growth of the longitudinal emittance ($\varepsilon_{long_{fin}}/\varepsilon_{long_{ini}}$) as a function of the initial root-mean-square energy and arrival time spreads after passage through one lithium rod for a fixed value of initial ε_{tr}. b. The region in which the antidamping process dominates over the fluctuation of ionization losses (in other words, the region where the growth of the longitudinal emittance is below a preassigned value defined from the asymptotics) for different values of the initial transverse emittance after passage through one lithium rod.

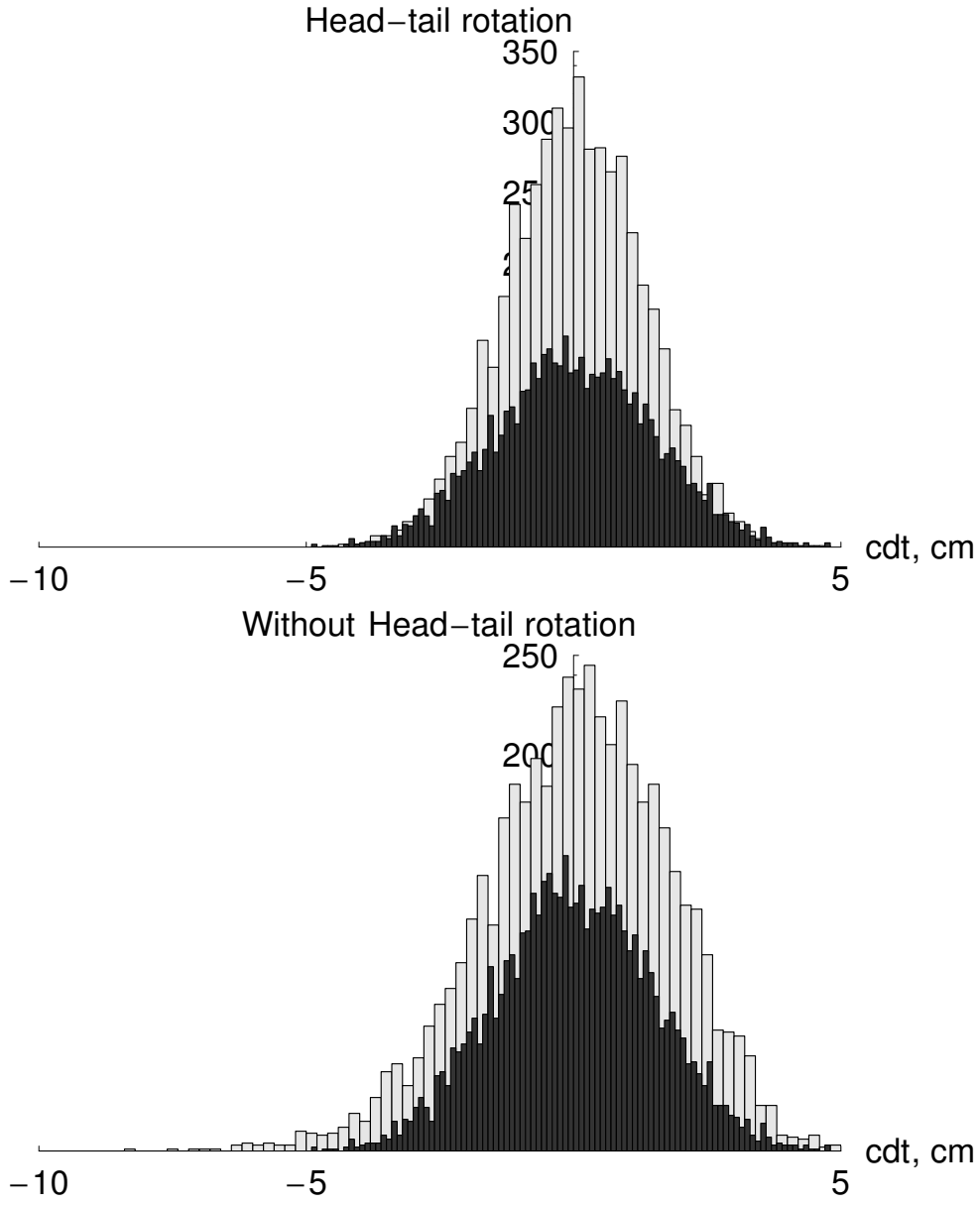

Figure 9: The evolution of the distribution of the arrival time spread after passing through 5 rods in cases of (top) "head-tail" rotation usage and (bottom) without it; ■ — initial distribution, □ — distribution after passing 5 rods.

result of the emergence of a long tail, is that the "center-of-gravity" of the distribution shifts from the peak position. All this means that non-paraxial particles lose more energy than those at the center, causing them to drop behind the main part of the beam. This emphasizes again the importance of taking transverse parameters into account during a study of longitudinal motion.

A similar analysis of the energy spread (Fig. 10 bottom) also shows particles with bigger losses, but the amount of distribution deformation is not as significant in this case.

It appears that a procedure of beam symmetrization ("head-tail" rotation (11)), consisting of beam rotation in longitudinal phase-space by an angle of π, can completely solve this problem; it allows one to obtain the same rate of longitudinal emittance growth in simulation as the linear model predicts without additional increase due to non-paraxiality effects. Similar simulations of the evolution of cdt and dE/E distributions but with with "head-tail" rotation usage are shown in the Fig. 9 (top) and 10 (top) respectively. Even just visually, the final distributions are much more symmetric and narrow. The beam symmetrization was simulated as a thin ideal process after the second and forth rods. Practically, it can be realized by an additional RF section with a zero acceleration gradient placed in each period of the cooling system (or performing an additional RF-gymnastic in sections of energy recovery). The influence of this procedure on a muon's lifetime and its technical parameters will be estimated in future work.

6. Summary

The motion of a muon beam in the final cooling scheme based on lithium rods has been simulated using LyRICS software. The analytical linearized model of muon beam motion, which helps to check the code of the developed software, was used to determine the influence of non-paraxiality and the interdependence of transverse and longitudinal motion. Preliminary estimations of the optimal longitudinal beam parameters for the emittance exchange procedure, which will possibly help to organize the cooling of all degrees of freedom, are presented in Section 5.1.

The main conclusions are:

1. The selected linear model is able to describe the transverse motion with high precision independent of beam longitudinal parameters (in the range reasonable for all parameters in this type of cooling).

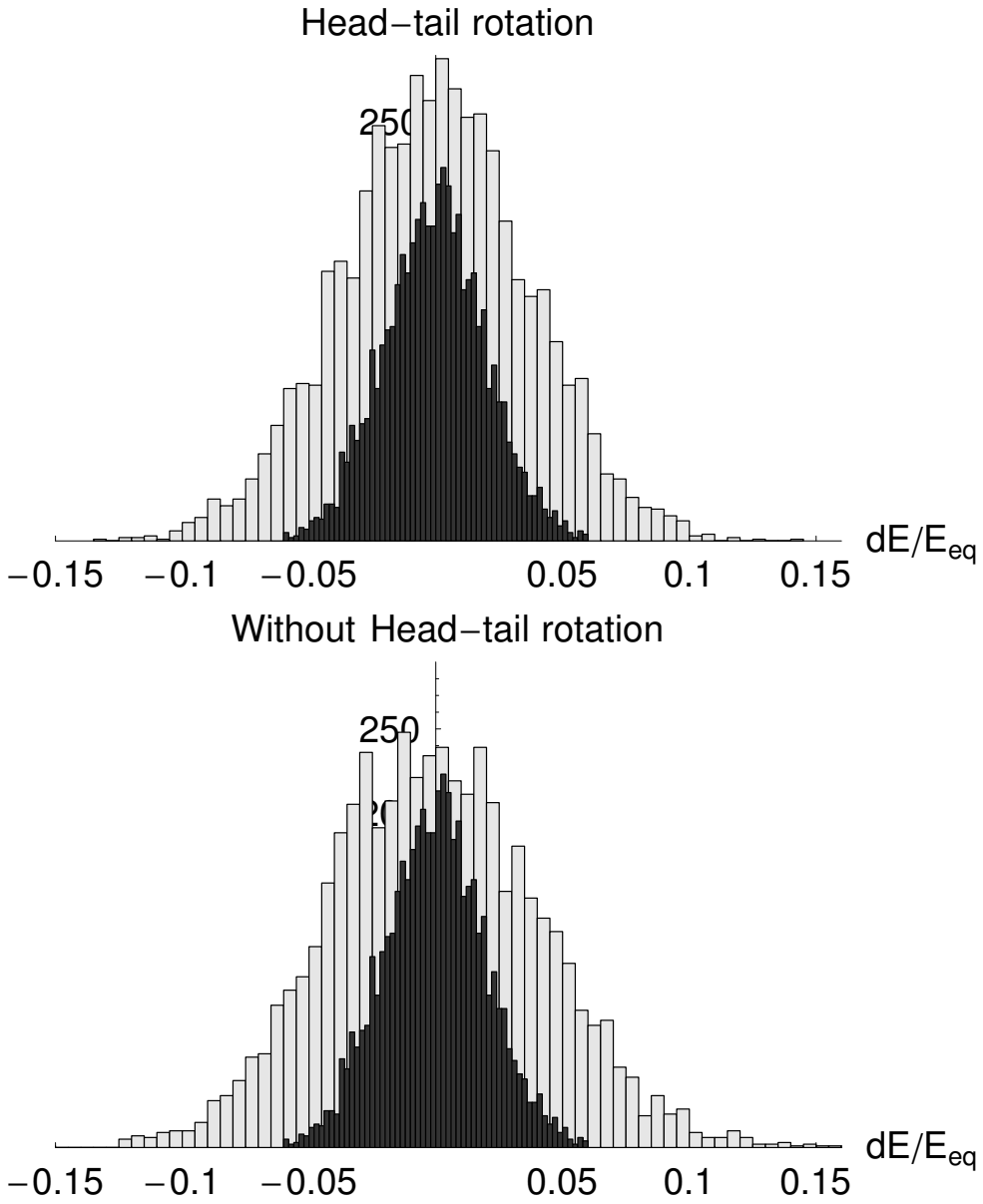

Figure 10: The evolution of the distribution of the relative energy spread after passing through 5 rods in cases of (top) "head-tail" rotation usage and (bottom) without it; ■ — initial distribution, □ — distribution after passing 5 rods.

2. The evolution of the relative energy deviation also converges with the linear model for a wide range of transverse emittances and is independent of the deviation in the arrival time. In contrast, the spread of the arrival time agrees with the linear model only in the case of small transverse emittance, which is a direct consequence of non-paraxiality (particles with large angular deviations follow a longer path in matter than the equilibrium one, which results in the "tail" formation in the direction of delayed particles). Also, the dependence of the root-mean-square arrival time on the transverse emittance makes the optimal beam longitudinal sizes (corresponding to a minimal increment of longitudinal heating) depend on it too.
3. The additional increase of the longitudinal emittance in comparison with the linear model prediction (which was detected in (11)) have been described in more detail. The statistical approach gives cogent evidence of the efficiency of the "head-tail" rotation procedure for suppression of non-paraxiality related effects.

7. Acknowledgment

We are grateful to S.I. Eidelman, V.V. Parkhomchuk, E.A. Perevedentsev and N.A. Vinokurov for useful discussions. Also we are grateful to P. McCall for proof reading the manuscript.

A. Linearized model of transverse motion

The transverse motion can be approximately described by a paraxial linear model with a fixed mean energy of a beam[2]. For a case of paraxial motion, it is simple to replace time derivatives to those over the longitudinal path in the equation of motion. Using notations in which operators $\frac{d}{dt}$ and $\frac{d}{ds}$ are denoted as $\dot{}$ and $'$, respectively, and neglecting a variation of the total mean velocity (which is applicable in this approach):

$$\begin{aligned}\frac{dp_x}{dt} &= \gamma_\mu m_\mu \frac{d}{dt}\left(\frac{dx}{ds}\underbrace{\frac{ds}{dt}}_{=v_\mu}\right) = \\ &= \gamma_\mu m_\mu \left(v_\mu \frac{d}{dt}\left(\frac{dx}{ds}\right) + x'\underbrace{\frac{d}{dt}v_\mu}_{=0}\right) = \\ &= \gamma_\mu m_\mu v_\mu \frac{dx'}{ds}\frac{ds}{dt} = \gamma_\mu \beta_\mu^2 m_\mu c^2 x''.\end{aligned}$$

The frictional force[3]

$$F_{fr_x} \approx F_{fr}x' = -(dE/dl)x'$$

and focusing force

$$F_{foc} = -e\beta_\mu G x,$$

where G is a field gradient, substituted into the equation of motion

$$\frac{d\mathbf{p}}{dt} = \sum_i \mathbf{F}_i, \tag{4}$$

[2]In reality it conforms to short enough sections with matter which alternate with sections of energy recovery.

[3]The dE/dl value of average friction forces due to ionization losses is characterized by the Bethe-Bloch equation (16):

$$-\frac{dE}{dl}(\beta_\mu) = \frac{4\pi n_e e^4}{m_e \beta_\mu^2 c^2}\left[\ln\frac{c\beta_\mu\gamma_\mu\sqrt{2m_e T_{max}}}{\bar{I}} - \beta_\mu^2\right], \tag{3}$$

where T_{max} is a maximal possible kinetic energy transferred to an electron in a single collision, I is a mean excitation energy and n_e is an electron density of matter.

without taking into account scattering, immediately result in a standard equation for damped oscillations for one of the transverse degrees of freedom:

$$x'' + 2\lambda_s x' + k_s^2 x = 0, \tag{5}$$

where λ_s and k_s are determined by:

$$\lambda_s = \frac{1}{2\gamma_\mu \beta_\mu^2 m_\mu c^2} \frac{dE}{dl}, \tag{6}$$

$$k_s = \sqrt{\frac{eG}{\gamma_\mu \beta_\mu m_\mu c^2}}. \tag{7}$$

Averaging over the ensemble makes it possible to rewrite the expression (5) as a system of linear differential equations in terms of beam second moments:

$$\begin{cases} \langle x^2 \rangle' &= 2\langle xx' \rangle \\ \langle xx' \rangle' &= \langle x'x' \rangle + \langle xx'' \rangle = \\ &= \langle x'^2 \rangle - k_s^2 \langle x^2 \rangle - 2\lambda_s \langle xx' \rangle \ . \\ \langle x'^2 \rangle' &= 2\langle x'x'' \rangle = \\ &= -2k_s^2 \langle xx' \rangle - 4\lambda_s \langle x'^2 \rangle \end{cases}$$

Converting it to a matrix form and adding the column corresponding to the scattering process omitted in (5), we have:

$$\begin{bmatrix} \langle x^2 \rangle \\ \langle xx' \rangle \\ \langle x'^2 \rangle \end{bmatrix}' = \begin{bmatrix} 0 & 2 & 0 \\ -k_s^2 & -2\lambda_s & 1 \\ 0 & -2k_s^2 & -4\lambda_s \end{bmatrix} \cdot \begin{bmatrix} \langle x^2 \rangle \\ \langle xx' \rangle \\ \langle x'^2 \rangle \end{bmatrix} + \begin{bmatrix} 0 \\ 0 \\ \Theta_x^2 \end{bmatrix}.$$

Two zeroes in an additional column describe a zero value of the average scattering angle and a fact that the scattering process does not produce immediate influence on a transverse coordinate. The value of Θ_x has a meaning of a root-mean-square scattering angle per unit of length passed in matter, which in the first approximation can be described by the expression for multiple Coulomb scattering (15):

$$\Theta_x^2 = \frac{4\pi n_e z^2 (Z+1) e^4}{\gamma_\mu^2 \beta_\mu^4 m_\mu^2 c^4} L_c, \tag{8}$$

where z and Z are charges of a scattered particle and scattering one, respectively (in elementary electron charge) and L_c is a Coulomb logarithm.

A solution of this equation is given by a sum of the general solution

$$\begin{aligned}
\langle x^2\rangle_{GS} &= e^{-2\lambda_s s}\left[C_1\frac{1}{k_s^2}+\right.\\
&\quad + C_2\left(\frac{2\lambda_s^2-k_s^2}{k_s^4}\cos 2\omega s-\frac{2\lambda_s}{k_s^2}\frac{\omega}{k_s^2}\sin 2\omega s\right)+\\
&\quad \left.+ C_3\left(\frac{2\lambda_s^2-k_s^2}{k_s^4}\sin 2\omega s+\frac{2\lambda_s}{k_s^2}\frac{\omega}{k_s^2}\cos 2\omega s\right)\right],\\
\langle xx'\rangle_{GS} &= e^{-2\lambda_s s}\left[-C_1\frac{\lambda_s}{k_s^2}+\right.\\
&\quad + C_2\left(-\frac{\lambda_s}{k_s^2}\cos 2\omega s+\frac{\omega}{k_s^2}\sin 2\omega s\right)+\\
&\quad \left.+ C_3\left(-\frac{\lambda_s}{k_s^2}\sin 2\omega s-\frac{\omega}{k_s^2}\cos 2\omega s\right)\right],\\
\langle x'^2\rangle_{GS} &= e^{-2\lambda_s s}\left[C_1+\right.\\
&\quad \left.+ C_2\cos 2\omega s+C_3\sin 2\omega s\right],
\end{aligned}$$

where $\omega=\sqrt{k_s^2-\lambda_s^2}$, and a partial one

$$\langle x^2\rangle_{PS} = \frac{\Theta_x^2}{4\lambda_s k_s^2}, \tag{9}$$

$$\langle xx'\rangle_{PS} = 0, \tag{10}$$

$$\langle x'^2\rangle_{PS} = \frac{\Theta_x^2}{4\lambda_s}. \tag{11}$$

A substitution of the initial conditions $\left(\langle x^2\rangle_0,\langle xx'\rangle_0,\langle x'^2\rangle_0\right)$ into a complete solution with $s=0$ determines arbitrary constants C_i:

$$\left\{\begin{array}{lcc}
C_1 &=& -\frac{2\lambda_s k_s^4\langle x^2\rangle_0+4\lambda_s^2 k_s^2\langle xx'\rangle_0+2\lambda_s k_s^2\langle x'^2\rangle_0-\Theta_x^2 k_s^2}{4\lambda_s(\lambda_s^2-k_s^2)}\\
C_2 &=& \frac{2k_s^4\langle x^2\rangle_0+4\lambda_s k_s^2\langle xx'\rangle_0+2\left(2\lambda_s^2-k_s^2\right)\langle x'^2\rangle_0-\Theta_x^2\lambda_s^2}{4\lambda_s(\lambda_s^2-k_s^2)}\\
C_3 &=& -\frac{4k_s^2\langle xx'\rangle_0+4\lambda_s\langle x'^2\rangle_0-\Theta_x^2}{4\lambda_s\sqrt{k_s^2-\lambda_s^2}}
\end{array}\right. .$$

From this expression, we can obtain a non-oscillatory solution for beam second moments as well as matched initial conditions for it by making C_2 and C_3 equal to zero:

$$\begin{cases} \langle xx' \rangle_0^M = \dfrac{\Theta_x^2 - 4\lambda_s k_s^2 \langle x^2 \rangle_0}{4k_s^2} \\ \langle x'^2 \rangle_0^M = k_s^2 \langle x^2 \rangle_0 \end{cases}, \tag{12}$$

$$\begin{cases} \langle x^2 \rangle^M = \left(\langle x^2 \rangle_0 - \dfrac{\Theta_x^2}{4\lambda_s k_s^2} \right) e^{-2\lambda_s s} + \dfrac{\Theta_x^2}{4\lambda_s k_s^2} \\ \langle xx' \rangle^M = -\left(\lambda_s \langle x^2 \rangle_0 - \dfrac{\Theta_x^2}{4k_s^2} \right) e^{-2\lambda_s s} \\ \langle x'^2 \rangle^M = \left(k_s^2 \lambda_s \langle x^2 \rangle_0 - \dfrac{\Theta_x^2}{4\lambda_s} \right) e^{-2\lambda_s s} + \dfrac{\Theta_x^2}{4\lambda_s} \end{cases}. \tag{13}$$

It seems that asymptotics of the complete solution is a partial solution (9) because of presence in the general solution of the exponentially damped factor. This asymptotics also gives the equilibrium value of the transverse emittance:

$$\varepsilon_{tr}^{eq} = \lim_{s \to \infty} \sqrt{\langle x^2 \rangle_{PS} \langle x'^2 \rangle_{PS} - \langle xx' \rangle_{PS}^2} = \frac{\Theta_x^2}{4\lambda_s k_s}. \tag{14}$$

B. Linearized model of longitudinal motion

Similarly to the model selected for the transverse motion, in a paraxial case one can describe the longitudinal motion of a test particle relative to the equilibrium one with an average beam energy. The time derivative of momentum in case when an acting force is directed along velocity

$$\frac{dp}{dt} = m_\mu \gamma_\mu^3 \dot{v},$$

substituted into (4), gives a differential equation of the second order (Newton equation)[4]:

$$\ddot{z}(t) = \frac{1}{m_\mu \gamma_\mu^3} F_{fr}.$$

[4]In contrast to A, for the longitudinal motion there is no focusing force when particles move in matter, which appears only in the section of energy recovery.

A full friction force F_{fr} can be represented as a sum of average losses (3) and stochastic force f responsible for fluctuations of average losses:

$$\ddot{z}\left(t\right)=\frac{1}{m_{\mu}\gamma_{\mu}^{3}}\left(-\frac{dE}{dl}+f(t)\right). \tag{15}$$

Having selected an equilibrium particle which moves with average velocity of a beam β_{eq}, and linearizing dE/dl as $\kappa\beta_{\mu}+b$ (Fig. 11), one can obtain the equation of motion for the equilibrium particle:

$$\ddot{z}_{eq}=-2\lambda_{t}\dot{z}_{eq}-\frac{b}{m_{\mu}\gamma_{\mu}^{3}}, \tag{16}$$

where

$$\lambda_{t}=\frac{\kappa c}{2m_{\mu}c^{2}\gamma_{\mu}^{3}}.$$

The set of (15) and (16) gives the equation for a deviation of a test particle from the equilibrium one:

$$\left(\ddot{z}-\ddot{z}_{eq}\right)=-2\lambda_{t}\left(\dot{z}-\dot{z}_{eq}\right)-f\left(t\right). \tag{17}$$

Turning it to a differential equation of the first order for a relative velocity, one obtains:

$$\Delta\dot{v}=-2\lambda_{t}\Delta v-f\left(t\right), \tag{18}$$

which solution is:

$$\Delta v\left(t\right)=\Delta v_{0}e^{-2\lambda_{t}t}-e^{-2\lambda_{t}t}\int\limits_{0}^{t}e^{2\lambda_{t}\tau}f\left(\tau\right)\,d\tau, \tag{19}$$

where $\Delta v_{0}=\Delta v|_{t=0}$ is the initial condition. Averaging over a stochastic

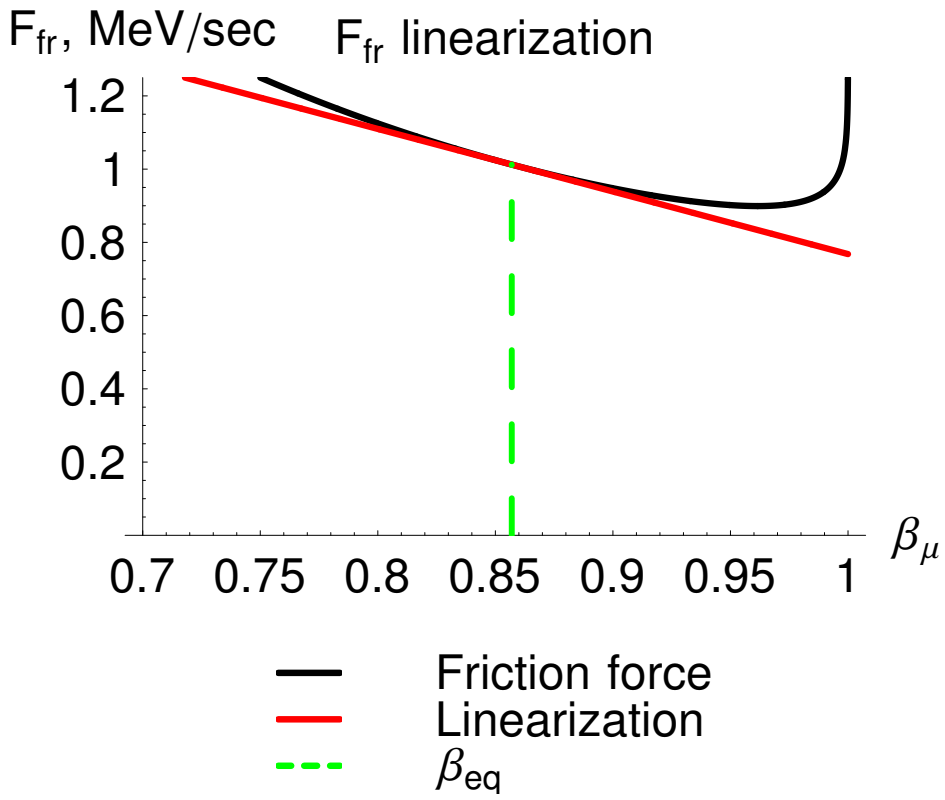

Figure 11: The average ionization losses and its linear approximation as a function of muon velocity.

force of (19) allows one to find the correlation function of velocity:

$$\begin{aligned}\langle \Delta v\left(t_1\right) \Delta v\left(t_2\right)\rangle_f = \\ = {\Delta v_0}^2 e^{-2\lambda_t t_1 - 2\lambda_t t_2} + e^{-2\lambda_t t_1 - 2\lambda_t t_2} \times \\ \times \int_0^{t_2}\int_0^{t_1} e^{2\lambda_t \tau_1 + 2\lambda_t \tau_2} \langle f\left(\tau_1\right) f\left(\tau_2\right)\rangle \, d\tau_1 d\tau_2 - \\ - \Delta v_0 e^{-2\lambda_t t_1} \int_0^{t_2} e^{2\lambda_t \tau_2} \langle f\left(\tau_2\right)\rangle \, d\tau_2 - \\ - \Delta v_0 e^{-2\lambda_t t_2} \int_0^{t_1} e^{2\lambda_t \tau_1} \langle f\left(\tau_1\right)\rangle \, d\tau_1.\end{aligned}$$

Considering the fluctuation of energy losses as a Gaussian stochastic process delta-correlated in time with a zero mean value (17):

$$\begin{cases} \langle f\left(t\right)\rangle = 0 \\ \langle f\left(t_1\right) f\left(t_2\right)\rangle = B\left(t_1, t_2\right) = B\delta\left(t_1 - t_2\right) \end{cases}, \tag{20}$$

and assuming $t_1 = t_2$, the root-mean-square velocity spread becomes[5]:

$$\langle \Delta v^2\left(t\right)\rangle_f = \left({\Delta v_0}^2 - \frac{B}{4\lambda_t}\right) e^{-4\lambda_t t} + \frac{B}{4\lambda_t}. \tag{21}$$

Making a similar proof for the value of the longitudinal deviation $\Delta z\left(t\right)$: writing a solution in an integrated form from $\Delta \dot{z} = \Delta v$

$$\Delta z\left(t\right) = \Delta z_0 + \int_0^t \Delta v\left(\tau\right) \, d\tau, \tag{22}$$

[5]Comparison of (21) and (13) shows the meaning of B — this is a root-mean-square velocity "spread" per unit time, arising because of fluctuations of energy losses:

$$\Theta^2_{dE/E} = 2\pi\beta_\mu c r_\mu n_e [2 - \beta^2_\mu],$$

from which

$$\Theta_v = B^{1/2} \simeq \frac{c}{\beta_\mu \gamma^2_\mu} \Theta_{dE/E}.$$

and averaging it by a stochastic force, one can find the root-mean-square value of $\Delta z\,(t)$:

$$\langle \Delta z^2\,(t)\rangle_f = \Delta z_0^2 + 2\Delta z_0 \int\limits_0^t \langle \Delta v\,(\tau)\rangle\, d\tau + \\ + \int\limits_0^t \int\limits_0^t \langle \Delta v\,(\tau_1)\,\Delta v\,(\tau_2)\rangle\, d\tau_1\, d\tau_2 = \\ = \Delta z_0^2 + 2\Delta z_0 \Delta v_0 \frac{\left(e^{2\lambda_t t}-1\right)}{2\lambda_t} e^{-2\lambda_t t} + \\ + \frac{\left(e^{2\lambda_t t}-1\right)^2}{4\lambda_t^2}\left(\Delta v_0^2 - \frac{\Theta_v^2}{4\lambda_t}\right) e^{-4\lambda_t t} + \\ + \frac{\left(e^{-\lambda_t t}-e^{\lambda_t t}\right)^2}{4\lambda_t^2}\frac{\Theta_v^2}{4\lambda_t}. \quad (23)$$

The calculation of the cross correlation function gives:

$$\langle \Delta z\,(t)\,\Delta v\,(t)\rangle_f = \Delta z_0 \langle \Delta v(t)\rangle_f + \\ + \int\limits_0^t \langle \Delta v\,(t)\,\Delta v\,(\tau)\rangle_f\, d\tau = \\ = \Delta z_0 \Delta v_0 e^{-2\lambda_t} + \frac{\left(e^{2\lambda_t t}-1\right)}{2\lambda_t}\frac{\Theta_v^2}{4\lambda_t} e^{-2\lambda_t} - \\ - \frac{\left(e^{-2\lambda_t t}-1\right)}{2\lambda_t}\left(\Delta v_0^2 - \frac{\Theta_v^2}{4\lambda_t}\right) e^{-2\lambda_t t}. \quad (24)$$

Finally, averaging over the initial ensemble of particles and turning to variables of arrival time[6] and energy deviation

$$\begin{cases} \Delta z \to \beta_{eq}\Delta z \approx c\Delta t \\ \Delta v \to \beta_{eq}\gamma_{eq}^2 \dfrac{\Delta v}{c} \approx \dfrac{\Delta E}{E_{eq}} \end{cases},$$

[6]Here and further multiplied by the speed of light c.

one can find an expression describing the behavior of the longitudinal emittance for a beam moving in matter:

$$\varepsilon_{long} = \sqrt{\left\langle (c\Delta t)^2 \right\rangle \left\langle \left(\frac{\Delta E}{E_{eq}}\right)^2 \right\rangle - \left\langle (c\Delta t)\left(\frac{\Delta E}{E_{eq}}\right)\right\rangle^2}, \tag{25}$$

$$\begin{aligned}
\left\langle (c\Delta t)^2 \right\rangle &= \left\langle (c\Delta t)^2 \right\rangle_0 + \\
&+ 2\frac{c}{\gamma_{eq}^2}\left\langle (c\Delta t)\left(\frac{\Delta E}{E_{eq}}\right)\right\rangle_0 \frac{e^{2\lambda_t t}-1}{2\lambda_t} e^{-2\lambda_t t} + \\
&+ \frac{c^2}{\gamma_{eq}^4}\frac{\left(e^{-\lambda_t t}-e^{\lambda_t t}\right)^2}{4\lambda_t^2}\frac{\Theta_{dE/E}^2}{4\lambda_t} + \\
&+ \frac{c^2}{\gamma_{eq}^4}\frac{\left(e^{2\lambda_t t}-1\right)^2}{4\lambda_t^2}\left(\left\langle \left(\frac{\Delta E}{E_{eq}}\right)^2 \right\rangle_0 - \frac{\Theta_{dE/E}^2}{4\lambda_t}\right) e^{-4\lambda_t t} \\
\left\langle \left(\frac{\Delta E}{E_{eq}}\right)^2 \right\rangle &= \frac{\Theta_{dE/E}^2}{4\lambda_t} + \\
&+ \left(\left\langle \left(\frac{\Delta E}{E_{eq}}\right)^2 \right\rangle_0 - \frac{\Theta_{dE/E}^2}{4\lambda_t}\right) e^{-4\lambda_t t} \\
\left\langle (c\Delta t)\left(\frac{\Delta E}{E_{eq}}\right)\right\rangle &= \left\langle (c\Delta t)\left(\frac{\Delta E}{E_{eq}}\right)\right\rangle_0 e^{-2\lambda_t t} + \\
&+ \frac{c}{\gamma_{eq}^2}\frac{e^{2\lambda_t t}-1}{2\lambda_t}\frac{\Theta_{dE/E}^2}{4\lambda_t} e^{-2\lambda_t t} - \\
&- \frac{c}{\gamma_{eq}^2}\frac{e^{-2\lambda_t t}-1}{2\lambda_t}\left(\left\langle \left(\frac{\Delta E}{E_{eq}}\right)^2 \right\rangle_0 - \frac{\Theta_{dE/E}^2}{4\lambda_t}\right) e^{-2\lambda_t t}
\end{aligned} \quad , \tag{26}$$

where $\left\langle (c\Delta t)^2 \right\rangle_0$, $\left\langle \left(\frac{\Delta E}{E_{eq}}\right)^2 \right\rangle_0$, $\left\langle (c\Delta t)\left(\frac{\Delta E}{E_{eq}}\right)\right\rangle_0$ are initial data averaged over the initial ensemble.

References

[1] Skrinsky A.N., "Ionization Cooling and Muon Collider", in Proceedings of 9-th ICFA Beam Dynamics Workshop: Beam Dynamics and Technology Issues for Muon-Muon Colliders, Montauk, NY (1995); *Nuclear*

Instruments and Methods in Physics Research Section A: Accelerators, Spectrometers, Detectors and Associated Equipment, Volume 391, 1997, Pages 188-195.

[2] Budker G.I., in Proceedings of the 7th International Conf. on High Energy Accelerators, Yerevan (1969) Page 33; extract in *Physics Potential and Development of* $\mu + \mu -$ *Colliders: Second Workshop*, ed. D. Cline, AIP Conf. Proc. 352, 4 (1996).

[3] Skrinsky A.N., presented at the International Seminar on Prospects of High-Energy Physics, Morges, 1971 (printed at CERN, unpublished); extract in *Physics Potential and Development of* $\mu + \mu -$ *Colliders: Second Workshop*, ed. D. Cline, AIP Conf. Proc. 352, 6 (1996).

[4] Bruning O., Collier P., "Building a Behemoth", *Nature*, Volume 448, 19 July 2007, Pages 285-289.

[5] Skrinsky A.N., Parkhomchuk V.V., *Sov. J. Part. Nucl.* 12, Pages 223-247 (1981).

[6] Skrinsky A.N., "Accelerator and Instrumentation Prospects of Elementary Particle Physics," in Proceedings of the XX International ("Rochester") Conference on High Energy Physics, Madison, 1980, New York, 1981, v.2, Pages 1056-1093; and in *Uspekhi Fiz. Nauk*, Moscow, 1982, 138, 1, Pages 3-43; translated at Soviet Physics Uspekhi 25 (9), September 1982, Pages 639-661.

[7] Skrinsky A.N., "Remarks on High Energy Muon Collider" in Muon Colliders at 10 Tev to 100 TeV (HEMC'99 Workshop), Montauk 1999; AIP Conference Proceedings, v. 530, 200, Pages 311-315.

[8] Palmer R.B., "Progress toward a Muon Collider" in Particle Accelerator Conference (PAC09), May 4-8 2009, Vancouver, Canada (author index TU1GRI03).

[9] Shiltsev V., "When Will We Know a Muon Collider is Feasible? Status And Directions of Muon Accelerator R&D", *Modern Physics Letters A*, Volume 25, No. 8, 2010, Pages 567-577.

[10] Geer S., *Annu. Rev. Nucl. Part. Sci.* 59, 347 (2009).

[11] Skrinsky A.N., Zolkin T.V.,"Conceptual design and the simulation of final cooling section for a muon collider", *Nuclear Instruments and Methods in Physics Research Section A: Accelerators, Spectrometers, Detectors and Associated Equipment*, Volume 608, Issue 1, 1 September 2009, Pages 42-47.

[12] Yonehara K. et. al.,"MANX, A 6-D Muon Beam Cooling Experiment for RAL" in Particle Accelerator Conference (PAC09), May 4-8 2009, Vancouver, Canada (author index WE6PFP090).

[13] Zisman M.S.,"R&D toward a Neutrino Factory and Muon Collider" in Particle Accelerator Conference (PAC09), May 4-8 2009, Vancouver, Canada (author index TU1GRI02).

[14] Palladino V.C.,"Status of the MICE Muon Ionization Cooling Experiment" in Particle Accelerator Conference (PAC09), May 4-8 2009, Vancouver, Canada (author index TU6RFP057).

[15] Muhin K.N., "The Experimental Nuclear Physics. The Physics of Atomic Nucleus", Textbook. in 3 v., V.1. 6th-ed., Sptb.: Publishing-house "Lan", Pages 297-328, (2008).

[16] Particle Physics Booklet, extracted from the *Review of Particle Physics*, C.Amsler et al., Physics Letters B667,1 (2008).

[17] Grupen C., "Particle Detectors", Cambridge University Press, 1996.